Pergamon

Int. J. Heat Mass Transfer. Vol. 41, No. 2, pp. 357–372, 1998

Printed in Great Britain
0017–9310/98 $19.00 + 0.00

PII: S0017-9310(97)00136-1

Transient free convection flow past a vertical flat plate subject to a sudden change in surface temperature

S. D. HARRIS, L. ELLIOTT and D. B. INGHAM†
Department of Applied Mathematical Studies, University of Leeds, Leeds LS2 9JT, U.K.

and

I. POP
Faculty of Mathematics, University of Cluj, R-3400 Cluj, CP 253, Romania

(*Received* 29 *April* 1997)

Abstract—The transient free convection boundary-layer flow of a viscous and incompressible fluid adjacent to a semi-infinite vertical flat plate is investigated. It is assumed that for time $\bar{t} < 0$ a steady state boundary-layer has been obtained in which there is a uniform temperature T_∞ at large distances from the plate and the plate is at a temperature T_1. Then at $\bar{t} = 0$ the temperature of the plate is suddenly changed to T_2 and maintained at this value for $\bar{t} > 0$. The solution is dependent upon two parameters, namely the ratio of the final temperature above ambient to the initial temperature above ambient, $R = \Delta T_2/\Delta T_1 = (T_2 - T_\infty)/(T_1 - T_\infty)$, and the Prandtl number Pr. An analytical solution is presented which is valid at small values of $\bar{t}$. A new phenomena in this class of problems that is obtained from the detailed numerical scheme is the existence of two solutions, only one of which is physically acceptable, to the finite-difference equations associated with the matching technique applied for times beyond that at which the step-by-step method breaks down. Results have been obtained for a range of values of the parameter R, when $Pr = 1$. © 1997 Elsevier Science Ltd.

1. INTRODUCTION

Transient free convection flows often exist in technological applications where devices are either heated or cooled. The applications include, for example, the cooling of the core of a nuclear reactor in the case of power or pump failures, and the warming and cooling of electronic components. This type of transient process was pioneered by Illingworth [1], who studied the simpler circumstance of transient free convection adjacent to an infinite isothermal flat vertical surface and his analysis has been very much refined and generalized since then.

Sugawara and Michiyoshi [2] were the first to present results of a numerical analysis for the transient free convection adjacent to a semi-infinite isothermal vertical flat plate and an estimate of the total time duration of the transient process was reported. Siegel [3] used the Kárman–Pohlhausen method to investigate a similar flow situation and the time duration of the one-dimensional conduction regime, as well as the total transient time were presented. The boundary-layer thickness was found to reach a maximum whilst the heat transfer coefficient was a minimum during the transient procedure. Hellums and Churchill [4] and Carnahan *et al.* [5] have also conducted a numerical study of this problem and shown that the effect of the leading edge propagates at a speed which is in excess of the maximum one-dimensional unsteady speed. Later, Ingham [6, 7] used four quite different numerical methods to solve this problem and concluded that all the results showed: (i) a departure from the unsteady one-dimensional solution before the theoretically predicted time, and (ii) as the mesh size decreases the progression from the unsteady solution to the steady state solution is quicker, but not by means of a smooth transition. In summary, it should be mentioned that there is a vast amount of literature on the subject of transient free convection adjacent to a vertical flat plate and comprehensive reviews are given by Gebhart [8, 9], Joshi [10] and more recently by Pop *et al.* [11].

In many industrial and environmental situations, transients do not start from quiescence, but from a previous heating and resulting flow condition. An example is a solar collector panel, when solar insulation suddenly changes, possibly due to changing cloud cover. An initial steady flow becomes a transition, which ultimately may result in another steady flow condition, as in the models of Ingham [12, 13], Joshi and Gebhart [14] and Harris *et al.* [15, 16].

The objective of the present paper is to perform a

† Author to whom correspondence should be addressed.

NOMENCLATURE

a value of $f_0''(0)$ required for the small time analysis
b value of $(-\theta_0'(0))$ required for the small time analysis
f non-dimensional, reduced streamfunction
F transformed function
$\mathscr{F}$ non-dimensional velocity function, $\partial f/\partial\eta$
G transformed temperature function
Gr_x local Grashof number based on the initial temperature difference ΔT_1
h step length in η-direction for $0 < \tau \leqslant \tau_n^*$
$\tilde{h}$ step length in η-direction for $\tau_n^* < \tau < \tau_\infty$
H_k^1 system of non-linear algebraic equations
H_k^2 system of linear algebraic equations
$\tilde{k}$ non-dimensional time increment for $\tau_n^* < \tau < \tau_\infty$
m number of grid spacings in the τ-direction for $\tau_n^* < \tau < \tau_\infty$
n number of grid spacings in the η-direction for $\tau_n^* < \tau < \tau_\infty$
N number of grid spacings in the η-direction for $0 < \tau \leqslant \tau_n^*$
p, q variable coefficients in the governing equation for $\tau_n^* < \tau < \tau_\infty$
Pr Prandtl number
R ratio of final characteristic temperature to initial characteristic temperature
S sum of numerical solutions for velocity functions over consecutive time steps
t sum of numerical solutions for temperature over consecutive time steps
T fluid temperature
T_1 initial constant wall temperature ($\bar{\tau} \leqslant 0$)
T_2 final constant wall temperature ($\bar{\tau} > 0$)
ΔT_1 characteristic temperature ($\bar{\tau} \leqslant 0$)
ΔT_2 characteristic temperature ($\bar{\tau} > 0$)
u, v velocity components along x- and y-axes, respectively
U_c characteristic velocity
x, y Cartesian coordinates along the plate and normal to it, respectively.

Greek symbols

β volumetric coefficient of thermal expansion
δ boundary-layer thickness
ε tolerances in the numerical schemes
η, ξ non-dimensional similarity variables
θ non-dimensional temperature function
Θ, Ω expressions defined in equations (37) and (46)
$\lambda_1, \lambda_2, \lambda_3$ expressions defined in equations (37) and (46)
ν kinematic viscosity
$\bar{\tau}$ time
τ non-dimensional time
$\tilde{\tau}$ value of τ at which the transfer to the step-by-step method in η takes place
$\Delta\tau$ non-dimensional time increment for $0 < \tau < \tau_n^*$
Φ non-dimensional velocity function, $\partial F/\partial\xi$
ψ streamfunction
ω relaxation parameter.

Subscripts

0 value at $\tau = 0$
i, j evaluated at the ith and jth nodal points in the η- and τ-directions, respectively
n actual numerical values achieved
p exact values predicted
w wall values
∞ ambient condition.

Superscripts

$*$ point where the step-by-step numerical solution breaks down
η associated with the step-by-step numerical solution in the η and τ variables
ξ associated with the step-by-step numerical solution in the ξ and τ variables.

detailed theoretical study of the transient free convection from an isothermal semi-infinite vertical flat plate when the general transient arises from a sudden change in the level of the temperature of the plate. A steady input temperature T_1 is changed at the time $\bar{\tau} = 0$ to a new steady level T_2 and is maintained at this value for $\bar{\tau} > 0$, whilst the ambient temperature is T_∞. First, an analytical solution is obtained, which is valid at small values of the non-dimensional time, $\tau \ll 1$, in a region close to the plate, i.e. in an inner layer, for the fluid velocity and temperature fields, as well as for the skin friction and the heat transfer rate at the plate. Then, a very detailed numerical solution of the full boundary-layer equations is presented for the whole transient from $\bar{\tau} = 0$ to the steady state, $\bar{\tau} \to \infty$, by using a modification of the step-by-step method

proposed by Merkin [17] in combination with a finite-difference method similar to that devised by Dennis [18]. The effects of the ratio $R = \Delta T_2/\Delta T_1 = (T_2 - T_\infty)/(T_1 - T_\infty)$ on the velocity and temperature fields together with the skin friction and the heat transfer rate at the plate are determined when the Prandtl number, $Pr = 1$. Other values of Pr, which are $\mathbf{O}(1)$, have been considered, but the general conclusions are the same as those obtained for $Pr = 1$ and, therefore, the results obtained have not been presented.

2. GOVERNING EQUATIONS

We consider the general transient free convection boundary-layer flow adjacent to a semi-infinite vertical flat plate which is in a fluid at temperature T_∞. The initial steady transport is the free convection along the plate placed in a viscous and incompressible fluid at a constant temperature T_∞ with the plate at a uniform temperature T_1. A transient begins when the temperature T_1 is suddenly changed at time $\bar{\tau} = 0$ to a new value T_2 and maintained at this value for $\bar{\tau} > 0$. With the usual boundary-layer and Boussinesq approximations [19], the governing equations for the transient response at $\bar{\tau} > 0$ are

$$\frac{\partial u}{\partial x} + \frac{\partial v}{\partial y} = 0 \tag{1}$$

$$\frac{\partial u}{\partial \bar{\tau}} + u\frac{\partial u}{\partial x} + v\frac{\partial u}{\partial y} = \nu\frac{\partial^2 u}{\partial y^2} + g\beta(T - T_\infty) \tag{2}$$

$$\frac{\partial T}{\partial \bar{\tau}} + u\frac{\partial T}{\partial x} + v\frac{\partial T}{\partial y} = \frac{\nu}{Pr}\frac{\partial^2 T}{\partial y^2} \tag{3}$$

where x and y are the Cartesian coordinates along the plate and normal to it, respectively, u and v are the fluid velocity components along the x- and y-axes, T is the fluid temperature, g is the acceleration due to gravity, ν is the kinematic viscosity, β is the volumetric coefficient of thermal expansion and the Prandtl number, Pr, is defined to be the ratio of the kinematic viscosity to the thermal diffusivity of the fluid.

For time $\bar{\tau} \leqslant 0$, the steady flow resulted from the uniform wall temperature T_1, while for $\bar{\tau} > 0$, the wall temperature is at the constant level T_2. Therefore, equations (1)–(3) have to be solved subject to the boundary conditions

$$\begin{aligned} &u(0, y, \bar{\tau}) = v(0, y, \bar{\tau}) = 0, \quad T(0, y, \bar{\tau}) = T_\infty \\ &u(x, 0, \tau) = v(x, 0, \bar{\tau}) = 0, \quad T(x, 0, \bar{\tau}) = T_2 \\ &u(x, \infty, \bar{\tau}) = 0, \quad T(x, \infty, \bar{\tau}) = T_\infty \end{aligned} \tag{4}$$

for $\bar{\tau} > 0$ and $0 \leqslant x, y \leqslant \infty$.

For $\bar{\tau} > 0$ the non-dimensional reduced streamfunction, f, and the reduced temperature function, θ, are introduced as

$$\psi = U_c(x)\delta(x) f(\eta, \tau), \quad \theta(\eta, \tau) = \frac{T - T_\infty}{\Delta T_1} \tag{5}$$

where

$$\eta = \frac{y}{\delta(x)}, \quad \tau = \frac{\nu\bar{\tau}}{(\delta(x))^2}, \quad \delta(x) = \frac{x}{Gr_x^{1/4}}$$

$$U_c(x) = \frac{\nu}{x}(Gr_x)^{1/2}, \quad \Delta T_1 = T_1 - T_\infty. \tag{6}$$

Further, η is the non-dimensional similarity variable, $\delta(x)$ is the boundary-layer thickness, $U_c(x)$ is the characteristic velocity, ΔT_1 is the characteristic temperature, $Gr_x = g\beta\Delta T_1 x^3/\nu^2$ is the local Grashof number based on the initial temperature difference ΔT_1 and ψ is the streamfunction defined in the usual way, namely $u = \partial\psi/\partial y$ and $v = -\partial\psi/\partial x$.

The equations governing the evolution of the functions $f(\eta, \tau)$ and $\theta(\eta, \tau)$ can be obtained by substituting expressions (5) into equations (1)–(3). It is found that these functions satisfy the pair of coupled equations:

$$\frac{\partial^3 f}{\partial \eta^3} + \left(-1 + \frac{1}{2}\tau\frac{\partial f}{\partial \eta}\right)\frac{\partial^2 f}{\partial \eta\,\partial \tau} + \left(\frac{3}{4}f - \frac{1}{2}\tau\frac{\partial f}{\partial \tau}\right)\frac{\partial^2 f}{\partial \eta^2} - \frac{1}{2}\left(\frac{\partial f}{\partial \eta}\right)^2 + \theta = 0 \tag{7}$$

$$\frac{1}{Pr}\frac{\partial^2 \theta}{\partial \eta^2} + \left(-1 + \frac{1}{2}\tau\frac{\partial f}{\partial \eta}\right)\frac{\partial \theta}{\partial \tau} + \left(\frac{3}{4}f - \frac{1}{2}\tau\frac{\partial f}{\partial \tau}\right)\frac{\partial \theta}{\partial \eta} = 0. \tag{8}$$

These equations are to be solved for $\tau > 0$, subject to the boundary conditions

$$\begin{aligned} &f(0, \tau) = 0, \quad \frac{\partial f}{\partial \eta}(0, \tau) = 0, \quad \theta(0, \tau) = \frac{\Delta T_2}{\Delta T_1}, \\ &\frac{\partial f}{\partial \eta}(\infty, \tau) = 0, \quad \theta(\infty, \tau) = 0 \end{aligned} \tag{9}$$

where $\Delta T_2 = T_2 - T_\infty$.

The transport phenomenon at $\tau = 0$ is steady and hence $f(\eta, 0) = f_0(\eta)$ and $\theta(\eta, 0) = \theta_0(\eta)$, say, so that, from equations (7) and (8), $f_0(\eta)$ and $\theta_0(\eta)$ satisfy the following coupled ordinary differential equations

$$f_0''' + \tfrac{3}{4}f_0 f_0'' - \tfrac{1}{2}f_0'^2 + \theta_0 = 0 \tag{10}$$

$$\theta_0'' + \tfrac{3}{4}Pr f_0\theta_0' = 0. \tag{11}$$

The boundary conditions associated with these equations follow as similar reductions of the expressions (9) and are given explicitly by

$$f_0(0) = f_0'(0) = 0, \quad \theta_0(0) = 1, \quad f_0'(\infty) = \theta_0(\infty) = 0 \tag{12}$$

where prime denotes differentiation with respect to η.

A common starting point for the discussion of tran-

sient problems is to examine their behaviour for small times. A study of this transient process then reveals some of the basic features of the full boundary-layer equations and also provides a framework against which to develop the general transient process. This is where we begin our investigation.

3. SMALL TIME SOLUTION, $\tau \ll 1$

In the early development of the flow these exists an inner boundary-layer for $\tau \ll 1$, which is described by equations (7) and (8). Outside this layer, the flow remains at the initial boundary-layer profile, as given by $f_0(\eta)$ and $\theta_0(\eta)$ in equations (10) and (11). Since the appropriate length scale for small times is the diffusion scale, $\tau^{1/2}$, we use the new independent variables ξ and τ and introduce the following definitions:

$$f(\eta,\tau) = 2\tau^{3/2}F(\xi,\tau), \quad \theta(\eta,\tau) = G(\xi,\tau), \quad \xi = \frac{\eta}{2\tau^{1/2}}. \tag{13}$$

Substituting these variables in equations (7) and (8) yields

$$\frac{1}{4}\frac{\partial^3 F}{\partial \xi^3} - \frac{\partial F}{\partial \xi} + \tau\left(-1+\frac{1}{2}\tau^2\frac{\partial F}{\partial \xi}\right)\frac{\partial^2 F}{\partial \xi\,\partial \tau} + \left(\frac{1}{2}\xi - \frac{1}{2}\tau^3\frac{\partial F}{\partial \tau}\right)\frac{\partial^2 F}{\partial \xi^2} + G = 0 \tag{14}$$

$$\frac{1}{4Pr}\frac{\partial^2 G}{\partial \xi^2} + \tau\left(-1+\frac{1}{2}\tau^2\frac{\partial F}{\partial \xi}\right)\frac{\partial G}{\partial \tau} + \left(\frac{1}{2}\xi - \frac{1}{2}\tau^3\frac{\partial F}{\partial \tau}\right)\frac{\partial G}{\partial \xi} = 0 \tag{15}$$

which have to be solved subject to the boundary (inner) conditions at the plate:

$$F(0,\tau) = 0, \quad \frac{\partial F}{\partial \xi}(0,\tau) = 0, \quad G(0,\tau) = \frac{\Delta T_2}{\Delta T_1}. \tag{16}$$

The transformation (13) is that used by Ingham [12, 13] for the corresponding problem of a suddenly cooled vertical flat plate.

The solution of equations (14) and (15) in the growing inner layer is taken to match with that of the outer steady boundary-layer governed by equations (10) and (11). However, the solution in the outer steady boundary-layer region may be approximated at small η by the series expansions

$$f_0(\eta) \sim \tfrac{1}{2}a\eta^2 - \tfrac{1}{6}\eta^3 + \tfrac{1}{24}b\eta^4 + \mathbf{O}(\eta^5),$$
$$\theta_0(\eta) \sim 1 - b\eta + \mathbf{O}(\eta^2) \tag{17}$$

where $a = f_0''(0)$ and $b = -\theta_0'(0)$ depend upon the value of Pr. These expressions for $f_0''(0)$ and $\theta_0'(0)$ are determined by solving equations (10) and (11) using the Nag routine D02HAF, an algorithm which solves two-point boundary-value problems for systems of first-order, ordinary differential equations using a Runge–Kutta–Merson method and a Newton iteration in a shooting and matching technique. Thus, we find $a = 0.908191$ and $b = 0.401033$ for $Pr = 1$ [12].

Substitution of the transformation (13) into equation (17) yields, for large values of ξ

$$F(\xi,\tau) \sim a\xi^2\tau^{-1/2} - \tfrac{2}{3}\xi^3 + \tfrac{1}{3}b\xi^4\tau^{1/2} + \mathbf{O}(\tau),$$
$$G(\xi,\tau) \sim 1 - 2b\xi\tau^{1/2} + \mathbf{O}(\tau). \tag{18}$$

The behaviour of the inner boundary-layer solution as $\xi \to \infty$ is to be matched with the steady outer layer solution $f_0(\eta)$ and $\theta_0(\eta)$. It is the form of the asymptotic expressions (18) which suggests in the first instance the appropriate perturbation solution for $\tau \ll 1$ as

$$F(\xi,\tau) = \tau^{-1/2}F_0(\xi) + F_1(\xi) + \tau^{1/2}F_2(\xi) + \mathbf{O}(\tau),$$
$$G(\xi,\tau) = G_0(\xi) + \tau^{1/2}G_1(\xi) + \mathbf{O}(\tau). \tag{19}$$

Substitution of these series expansions into equations (14) and (15) and equating the terms of the same powers of τ gives rise to

$$\begin{aligned} F_0''' + 2\xi F_0'' - 2F_0' &= 0 \\ G_0'' + 2Pr\xi G_0' &= 0 \\ F_1''' + 2\xi F_1'' - 4F_1' &= -4G_0 \\ G_1'' + 2Pr\xi G_1' - 2PrG_1 &= 0 \\ F_2''' + 2\xi F_2'' - 6F_2' &= -4G_1 \\ &\vdots \end{aligned} \tag{20}$$

where primes denote differentiation with respect to ξ. Equation (20) must be solved subject to the following boundary conditions and asymptotic solutions:

$$F_i(0) = F_i'(0) = G_i(0) = 0, \quad i = 1,2,3,\ldots,$$
$$F_0(0) = F_0'(0) = 0, \quad G_0(0) = \frac{\Delta T_2}{\Delta T_1}$$
$$F_0(\xi) \sim a\xi^2, \quad F_1(\xi) \sim -\tfrac{2}{3}\xi^3,$$
$$F_2(\xi) \sim \tfrac{1}{3}b\xi^4, \ldots, \quad \text{as } \xi \to \infty$$
$$G_0(\xi) \sim 1, \quad G_1(\xi) \sim -2b\xi, \ldots, \quad \text{as } \xi \to \infty. \tag{21}$$

The solutions for F_i and G_i have been obtained in closed form for $i = 0$, 1 and 2 and therefore the resulting expressions for the velocity, $\partial F/\partial \xi$, and temperature, G, profiles may be readily established as

$$\frac{\partial F}{\partial \xi} = 2a\xi\tau^{-1/2} + \frac{1}{Pr-1}\left(1-\frac{\Delta T_2}{\Delta T_1}\right) \times \left[(1+2Pr\xi^2)\operatorname{erfc}(\sqrt{Pr}\xi) - 2\xi\sqrt{\frac{Pr}{\pi}}e^{-Pr\xi^2} - (1+2\xi^2)\operatorname{erfc}(\xi) + 2\xi\frac{1}{\sqrt{\pi}}e^{-\xi^2}\right] - 2\xi^2 + \frac{4}{3}b\xi^3\tau^{1/2} + \mathbf{O}(\tau) \tag{22}$$

$$G = 1-\left(1-\frac{\Delta T_2}{\Delta T_1}\right)\operatorname{erfc}(\sqrt{Pr}\,\xi)-2b\xi\tau^{1/2}+\mathbf{O}(\tau) \tag{23}$$

where the limiting value of the expression (22) for $\partial F/\partial\xi$ as $Pr \to 1$ is given by

$$\frac{\partial F}{\partial \xi} = 2a\xi\tau^{-1/2}+2\left(1-\frac{\Delta T_2}{\Delta T_1}\right) \times\left[\xi^2\operatorname{erfc}(\xi)-\xi\frac{1}{\sqrt{\pi}}\mathrm{e}^{-\xi^2}\right] -2\xi^2+\frac{4}{3}b\xi^3\tau^{1/2}+\mathbf{O}(\tau) \tag{24}$$

and $\operatorname{erfc}(\xi) = (2/\sqrt{\pi})\int_\xi^\infty \mathrm{e}^{-t^2}\,\mathrm{d}t$ is the complementary error function.

Expressions (22)–(24) are only applicable when $\eta \ll 1$, i.e. in the inner boundary-layer region. Small time solutions which are valid for all values of η are obtained by first writing equations (22)–(24) in terms of η and, subsequently, combining them with the outer solutions $f_0(\eta)$ and $\theta_0(\eta)$. The resulting velocity, $\partial f/\partial\eta$, and temperature, θ, profiles are thus given by

$$\frac{\partial f}{\partial \eta} = \frac{\mathrm{d}f_0}{\mathrm{d}\eta}+\frac{1}{Pr-1}\left(1-\frac{\Delta T_2}{\Delta T_1}\right) \times\left[\left(\tau+\frac{1}{2}Pr\eta^2\right)\operatorname{erfc}\left(\sqrt{Pr}\frac{\eta}{2\tau^{1/2}}\right) -\eta\tau^{1/2}\sqrt{\frac{Pr}{\pi}}\mathrm{e}^{-Pr(\eta^2/4\tau)} -\left(\tau+\frac{1}{2}\eta^2\right)\operatorname{erfc}\left(\frac{\eta}{2\tau^{1/2}}\right) +\eta\tau^{1/2}\frac{1}{\sqrt{\pi}}\mathrm{e}^{-\eta^2/4\tau}\right]+\mathbf{O}(\tau) \tag{25}$$

$$\theta = \theta_0-\left(1-\frac{\Delta T_2}{\Delta T_1}\right)\operatorname{erfc}\left(\sqrt{Pr}\frac{\eta}{2\tau^{1/2}}\right)+\mathbf{O}(\tau^{1/2}) \tag{26}$$

where the limiting value of the expression (25) for $\partial f/\partial\eta$ as $Pr \to 1$ is given by

$$\frac{\partial f}{\partial \eta} = \frac{\mathrm{d}f_0}{\mathrm{d}\eta}+\left(1-\frac{\Delta T_2}{\Delta T_1}\right)\left[\frac{1}{2}\eta^2\operatorname{erfc}\left(\frac{\eta}{2\tau^{1/2}}\right) -\eta\tau^{1/2}\frac{1}{\sqrt{\pi}}\mathrm{e}^{-\eta^2/4\tau}\right]+\mathbf{O}(\tau) \tag{27}$$

at small times τ.

Important physical quantities are also the non-dimensional skin friction coefficient on the plate, $\partial^2 f/\partial\eta^2|_{\eta=0}$, and the non-dimensional heat transfer on the plate, $\partial\theta/\partial\eta|_{\eta=0}$, as functions of τ. At small times these quantities have the following explicit series expansions:

$$\left.\frac{\partial^2 f}{\partial \eta^2}\right|_{\eta=0} = a-\frac{2}{\sqrt{\pi}}\frac{1}{\sqrt{Pr}+1}\left(1-\frac{\Delta T_2}{\Delta T_1}\right)\tau^{1/2}+\mathbf{O}(\tau) \tag{28}$$

$$q_w(\tau) = \left.\frac{\partial\theta}{\partial\eta}\right|_{\eta=0} = -b+\sqrt{\frac{Pr}{\pi}}\left(1-\frac{\Delta T_2}{\Delta T_1}\right)\tau^{-1/2}+\mathbf{O}(\tau^0). \tag{29}$$

4. NUMERICAL TECHNIQUES

Precise details in the transition range between small and large value of τ can only be obtained by a full numerical solution of the governing equations (7) and (8) under the boundary conditions (9). Furthermore, the range of validity of asymptotic estimates can only be assessed in comparison to exact numerical solutions. In pursuing such complete numerical solutions advantage can, however, be taken of the clearly established limiting solutions at small τ and at steady state $\tau = 0$ and $\tau = \infty$. Equations (7) and (8) are solved numerically for representative values of the non-dimensional parameter R and Prandtl number, $Pr = 1$. The method we use is a modification of that described by Merkin [17] in combination with the one first proposed by Dennis [18] for the solution of the boundary-layer equations. This method was also recently used by Harris *et al.* [15, 16] for the solution of transient free convection adjacent to a vertical surface embedded in a fluid-saturated porous medium. The method has to be modified to take care of the somewhat different momentum boundary-layer equations and boundary conditions, but this causes no extra computational difficulties.

The evolution of the pairs of functions $\partial F/\partial\xi$, G and $\partial f/\partial\eta$, θ are separately governed by the pairs of coupled partial differential equations (14), (15) and (7), (8), respectively, which are each parabolic and thus can be integrated numerically using a step-by-step method similar to that described by Merkin [17], provided that the coefficients of $\partial^2 F/\partial\xi\,\partial\tau$, $\partial G/\partial\tau$, $\partial^2 f/\partial\eta\,\partial\tau$ and $\partial\theta/\partial\tau$ all remain positive throughout the solution domain. This marching method enables the solution described by the functions $f_0(\eta)$, $\theta_0(\eta)$ at time $\tau = 0$ to proceed in time and gives a complete solution for $\tau \leqslant \tau_n^*$, where τ_n^* is the maximum value of τ reached in the numerical scheme, which is less than the precise time τ_p^* satisfying

$$\frac{1}{2}(\tau_p^*)^2\frac{\partial F}{\partial\xi}(0,\tau_p^*) = \frac{1}{2}\tau_p^*\frac{\partial f}{\partial\eta}(0,\tau_p^*) = 1. \tag{30}$$

The application of the step-by-step scheme to the pair of coupled equations (14) and (15) enables the accurate evolution of the temperature and velocity profiles to be determined over a developing inner layer whose width is increasing with time. If ξ_∞ and η_∞ are interpreted as being finite values of the spatial

variables at which the associated boundary conditions are to be applied, then at the exact time $\tilde{\tau}_p = (\eta_\infty/2\xi_\infty)^2$ we must transfer to the step-by-step scheme applied to equations (7) and (8). We again adopt the notation $\tilde{\tau}_n$ to denote the corresponding value of τ which is reached in our numerical techniques. Clearly, the appropriate values of ξ_∞ and η_∞ will establish a critical value of the parameter R above which $\tau_p^* \leqslant \tilde{\tau}_p$ so that the marching method breaks down before the transfer to the solution in the η, τ variables takes place.

The matching of the solution at $\tau = \tau_n^*$ to the asymptotic steady state solution may now be achieved using a variation of the method first described by Dennis [18].

4.1. *Numerical solution for* $0 < \tau \leqslant \tilde{\tau}_n$

The evolution of the velocity function, $\Phi = \partial F/\partial\xi$, and the temperature function, G, are governed by the coupled integro-differential equations

$$\tau\left(1-\frac{1}{2}\tau^2\Phi\right)\frac{\partial\Phi}{\partial\tau} = \frac{1}{4}\frac{\partial^2\Phi}{\partial\xi^2} + \frac{\partial\Phi}{\partial\xi}\left[\frac{1}{2}\xi - \frac{1}{2}\tau^3\int_0^\xi \frac{\partial\Phi}{\partial\tau}(\xi',\tau)\,\mathrm{d}\xi'\right] - \Phi + G \quad (31)$$

$$\tau\left(1-\frac{1}{2}\tau^2\Phi\right)\frac{\partial G}{\partial\tau} = \frac{1}{4Pr}\frac{\partial^2 G}{\partial\xi^2} + \frac{\partial G}{\partial\xi}\left[\frac{1}{2}\xi - \frac{1}{2}\tau^3\int_0^\xi \frac{\partial\Phi}{\partial\tau}(\xi',\tau)\,\mathrm{d}\xi'\right] \quad (32)$$

which have to be solved subject to the boundary conditions:

$$\Phi(0,\tau) = 0, \quad G(0,\tau) = R \quad (33)$$

where the condition $F(0,\tau) = 0$ has been incorporated in equations (31) and (32), the conditions as $\xi \to \infty$:

$$\Phi(\xi_\infty,\tau) = \frac{1}{\tau}\frac{\mathrm{d}f_0}{\mathrm{d}\eta}(2\xi_\infty\sqrt{\tau}), \quad G(\xi_\infty,\tau) = \theta_0(2\xi_\infty\sqrt{\tau}) \quad (34)$$

where the undisturbed state remains, and the initial solution throughout the solution domain given by evaluating the profiles (22)–(24) at the small time $\tau = \tau_0$. In order to proceed with a numerical analysis of equations (31) and (32), the ξ space under investigation has been restricted to finite dimensions by regarding $\xi = \xi_\infty$ to correspond to $\xi = \infty$.

The finite spatial domain is divided into N^ξ equal grid spacings of length $h^\xi = \xi_\infty/N^\xi$. A variable time step is used and the value of this time step at the start of the jth time increment is denoted by $\Delta\tau_j$. We also introduce the notation $\Phi_{i,j}$, $G_{i,j}$ to represent the finite-difference approximations to the non-dimensional velocity function Φ and the temperature function G at the point $\xi = (i-1)h^\xi$ for some time $\tau = \tau_j$.

Given a complete solution for $\Phi_{i,j}$, $G_{i,j}$ $i = 1, \ldots, N^\xi+1$, at time τ_j we require the solution for $\Phi_{i,j+1}$, $G_{i,j+1}$ at time $\tau = \tau_{j+1} = \tau_j + \Delta\tau_j$ and adopt the step-by-step finite-difference procedure described by Merkin [17]. This method involves first approximating the time derivatives by central differences and the remaining terms by their averages over the jth and $(j+1)$th time steps. Central differences are then introduced to estimate the spatial derivatives and the integrals in equations (31) and (32) are estimated using quadrature formulae following from the trapezium rule. Thus the finite-difference equations

$$\begin{aligned} &S^\xi_{i+1,j+\frac{1}{2}} - 2S^\xi_{i,j+1/2} + S^\xi_{i-1,j+1/2} \\ &\quad + 2(h^\xi)^2(\lambda_2 S^\xi_{i,j+1/2} - 4\lambda_1)(S^\xi_{i,j+1/2} - 2\Phi_{i,j}) \\ &\quad - 4(h^\xi)^2 S^\xi_{i,j+1/2} + 4(h^\xi)^2 t^\xi_{i,j+1/2} \\ &\quad + (h^\xi)^2(S^\xi_{i+1,j+1/2} - S^\xi_{i-1,j+1/2}) \\ &\quad \times [(i-1) - \lambda_2(\Omega^\xi_{i,j+1/2} - 2\Theta^\xi_{i,j})] = 0 \end{aligned} \quad (35)$$

$$\begin{aligned} &t^\xi_{i+1,j+1/2} - 2t^\xi_{i,j+1/2} + t^\xi_{i-1,j+1/2} \\ &\quad + 2Pr(h^\xi)^2(\lambda_2 S^\xi_{i,j+1/2} - 4\lambda_1)(t^\xi_{i,j+1/2} - 2G_{i,j}) \\ &\quad + Pr(h^\xi)^2(t^\xi_{i+1,j+1/2} - t^\xi_{i-1,j+1/2}) \\ &\quad \times [(i-1) - \lambda_2(\Omega^\xi_{i,j+1/2} - 2\Theta^\xi_{i,j})] = 0 \end{aligned} \quad (36)$$

represent approximations to the integro-differential equations (31) and (32) evaluated at $\xi = (i-1)h^\xi$ and $\tau = \tau_j + \frac{1}{2}\Delta\tau_j$, where

$$S^\xi_{i,j+1/2} = \Phi_{i,j+1} + \Phi_{i,j}, \qquad t^\xi_{i,j+1/2} = G_{i,j+1} + G_{i,j},$$

$$\Omega^\xi_{i,j+1/2} = \frac{1}{2}(S^\xi_{1,j+1/2} + S^\xi_{i,j+1/2}) + \sum_{i'=2}^{i-1} S^\xi_{i',j+1/2}$$

$$\lambda_1 = \frac{\tau_j}{\Delta\tau_j} + \frac{1}{2}, \quad \lambda_2 = \lambda_1^3(\Delta\tau_j)^2,$$

$$\Theta^\xi_{i,j} = \frac{1}{2}(\Phi_{1,j} + \Phi_{i,j}) + \sum_{i'=2}^{i-1}\Phi_{i',j}. \quad (37)$$

The boundary conditions (33) and (34) require that

$$S^\xi_{1,j+1/2} = 0,$$

$$S^\xi_{N^\xi+1,j+1/2} = \frac{1}{\tau_j}\frac{\mathrm{d}f_0}{\mathrm{d}\eta}(2\xi_\infty\sqrt{\tau_j}) + \frac{1}{\tau_j+\Delta\tau_j}\frac{\mathrm{d}f_0}{\mathrm{d}\eta}(2\xi_\infty\sqrt{\tau_j+\Delta\tau_j})$$

$$t^\xi_{1,j+1/2} = 2\frac{\Delta T_2}{\Delta T_1},$$

$$t^\xi_{N^\xi+1,j+1/2} = \theta_0(2\xi_\infty\sqrt{\tau_j}) + \theta_0(2\xi_\infty\sqrt{\tau_j+\Delta\tau_j}). \quad (38)$$

The system of non-linear algebraic equations $H^1_k(S^\xi_{2,j+1/2}, \ldots, S^\xi_{N^\xi,j+1/2}, t^\xi_{2,j+1/2}, \ldots, t^\xi_{N^\xi,j+1/2}) = 0$ and the system of algebraic equations $H^2_k(S^\xi_{2,j+1/2}, \ldots, S^\xi_{N^\xi,j+1/2}, t^\xi_{2,j+1/2}, \ldots, t^\xi_{N^\xi,j+1/2}) = 0$ comprising equations (35) and (36), respectively, thus define a set of $2(N^\xi-1)$ equations for $2(N^\xi-1)$ unknowns. If $S^{\xi(0)}_{i,j+1/2}$ and $t^{\xi(0)}_{i,j+1/2}$ are initial approxi-

mations to the solutions of these systems, we firstly determine a better approximation for $S^{\xi}_{i,j+1/2}$ by solving the system H^1_k. By employing Newton's method we can derive the following system of $(N^{\xi}-1)$ linear equations

$$\sum_{i=1}^{N^{\xi}}(S^{\xi}_{i,j+1/2}-S^{\xi(0)}_{i,j+1/2})\left(\frac{\partial H^1_k}{\partial S^{\xi}_{i,j+1/2}}\right)^{(0)} = -H^1_k(S^{\xi(0)}_{1,j+1/2},\ldots,S^{\xi(0)}_{N^{\xi},j+1/2},t^{\xi(0)}_{1,j+1/2},\ldots,t^{\xi(0)}_{N^{\xi},j+1/2}) \tag{39}$$

whose solution is achieved by decomposing the Jacobian matrix $\mathbf{J}_{ki}=(\partial H^1_k/\partial S^{\xi}_{i,j+1/2})^{(0)}$ into the product $\mathbf{J}=\mathbf{LU}$ of a lower-triangular matrix $\mathbf{L}$ and an upper-triangular matrix $\mathbf{U}$ using the method proposed by Doolittle and presented in Burden and Faires [20]. Thus the inversion of the linear system reduces to the separate solution of the two systems involving the matrices $\mathbf{L}$ and $\mathbf{U}$ by direct and backward substitution, respectively. Using this new estimate for $S^{\xi}_{i,j+1/2}$, the solution of the system of equations H^2_k provides the next approximation for $t^{\xi}_{i,j+1/2}$. This linear system can be inverted using the Thomas algorithm for tri-diagonal matrices applied to the associated matrix form of the equations H^2_k. This iterative process is repeated until the absolute difference between successive approximations for $S^{\xi}_{i,j+1/2}$ and $t^{\xi}_{i,j+1/2}$ reach values less than some tolerance ε^1_1 and ε^2_1, respectively.

The initial time increment $\Delta\tau_0$ at time $\tau=\tau_0$ is set to some prescribed small value and a time step doubling procedure is adopted. Given a complete solution at time τ_j and a previous time step $\Delta\tau_{j-1}$ the solution at time $\tau=\tau_j+2\Delta\tau_{j-1}$ is first calculated using the time increment $2\Delta\tau_{j-1}$ and then using two separate time increments of length $\Delta\tau_{j-1}$. If the absolute difference between the two solutions for $S^{\xi}_{i,j+1/2}$ and $t^{\xi}_{i,j+1/2}$ obtained at τ_{j+1} are separately less than the pre-assigned tolerances ε^1_2 and ε^2_2, respectively, then the time step is doubled so that $\Delta\tau_j=2\Delta\tau_{j-1}$. Otherwise the time increment remains unchanged.

4.2. *Numerical solution for* $\tau_n<\tau\leqslant\tau^*_n$

The evolution of the velocity function, $\mathscr{F}=\partial f/\partial\eta$, and the temperature function, θ, are governed by the coupled integro-differential equations

$$\left(1-\frac{1}{2}\tau\mathscr{F}\right)\frac{\partial\mathscr{F}}{\partial\tau}=\frac{\partial^2\mathscr{F}}{\partial\eta^2}+\frac{\partial\mathscr{F}}{\partial\eta}\int_0^{\eta}\left(\frac{3}{4}\mathscr{F}(\eta',\tau)-\frac{1}{2}\tau\frac{\partial\mathscr{F}}{\partial\tau}(\eta',\tau)\right)d\eta'-\frac{1}{2}\mathscr{F}^2+\theta \tag{40}$$

$$\left(1-\frac{1}{2}\tau\mathscr{F}\right)\frac{\partial\theta}{\partial\tau}=\frac{1}{Pr}\frac{\partial^2\theta}{\partial\eta^2}+\frac{\partial\theta}{\partial\eta}\int_0^{\eta}\left(\frac{3}{4}\mathscr{F}(\eta',\tau)-\frac{1}{2}\tau\frac{\partial\mathscr{F}}{\partial\tau}(\eta',\tau)\right)d\eta' \tag{41}$$

which have to be solved subject to the initial and boundary conditions:

$$\mathscr{F}(\eta,\tau_n)=\tau\Phi(\xi,\tau_n)|_{\xi=\eta/2\tau_n^{1/2}},\quad \theta(\eta,\tau_n)=G(\xi,\tau_n)|_{\xi=\eta/2\tau_n^{1/2}},\quad \mathscr{F}(0,\tau)=0,\quad \theta(0,\tau)=R \tag{42}$$

where the condition $f(0,\tau)=0$ has been incorporated in equations (40) and (41), and the conditions as $\eta\to\infty$:

$$\mathscr{F}(\eta_\infty,\tau)=0,\quad \theta(\eta_\infty,\tau)=0 \tag{43}$$

where the precise value of η_∞ is given by explicitly evaluating the expression $\eta_\infty=2\xi_\infty\tau_n^{1/2}$.

The finite spatial domain is divided into N^{η} equal grid spacings of length $h^{\eta}=\eta_\infty/N^{\eta}$. The variable time step and associated time step doubling procedure described in Section 4.1 are again used, subject to the error tolerances ε^1_4 and ε^2_4 associated with the solutions for $\mathscr{F}$ and θ, respectively. The notation $\mathscr{F}_{i,j}$, $\theta_{i,j}$ will be used to represent the finite-difference approximations to the non-dimensional velocity function $\mathscr{F}$ and the temperature function θ at the point $\eta=(i-1)h^{\eta}$ for some time $\tau=\tau_j$.

Employing the step-by-step procedure similar to that devised by Merkin [17], and described in Section 4.1, we thus obtain the following finite-difference equations:

$$\begin{aligned}&S^{\eta}_{i+1,j+1/2}-2S^{\eta}_{i,j+1/2}+S^{\eta}_{i-1,j+1/2}+2(h^{\eta})^2\left(\frac{1}{4}\lambda_1 S^{\eta}_{i,j+1/2}-\frac{1}{\Delta\tau_j}\right)\times(S^{\eta}_{i,j+1/2}-2\mathscr{F}_{i,j})+(h^{\eta})^2t^{\eta}_{i,j+1/2}\\&-\frac{1}{4}(h^{\eta})^2(S^{\eta}_{i,j+1/2})^2+(h^{\eta})^2(S^{\eta}_{i+1,j+1/2}-S^{\eta}_{i-1,j+1/2})\left[\lambda_3\Omega^{\eta}_{i,j+1/2}+\frac{1}{2}\lambda_1\Theta^{\eta}_{i,j}\right]=0\end{aligned} \tag{44}$$

$$\begin{aligned}&t^{\eta}_{i+1,j+1/2}-2t^{\eta}_{i,j+1/2}+t^{\eta}_{i-1,j+1/2}+2Pr(h^{\eta})^2\left(\frac{1}{4}\lambda_1 S^{\eta}_{i,j+1/2}-\frac{1}{\Delta\tau_j}\right)(t^{\eta}_{i,j+1/2}-2\theta_{i,j})\\&+Pr(h^{\eta})^2(t^{\eta}_{i+1,j+1/2}-t^{\eta}_{i-1,j+1/2})\times\left[\lambda_3\Omega^{\eta}_{i,j+1/2}+\frac{1}{2}\lambda_1\Theta^{\eta}_{i,j}\right]=0\end{aligned} \tag{45}$$

representing approximations to the integro-differential equations (40) and (41) evaluated at $\eta=(i-1)h^{\eta}$ and $\tau=\tau_j+\frac{1}{2}\Delta\tau_j$, where

$$S^{\eta}_{i,j+1/2}=\mathscr{F}_{i,j+1}+\mathscr{F}_{i,j},\quad t^{\eta}_{i,j+1/2}=\theta_{i,j+1}+\theta_{i,j},$$

$$\Omega^{\eta}_{i,j+1/2}=\frac{1}{2}(S^{\eta}_{1,j+1/2}+S^{\eta}_{i,j+1/2})+\sum_{i'=2}^{i-1}S^{\eta}_{i',j+1/2}$$

$$\lambda_3 = \frac{3}{16} - \frac{1}{4}\lambda_1, \quad \Theta^{\eta}_{i,j} = \frac{1}{2}(\mathscr{F}_{1,j} + \mathscr{F}_{i,j}) + \sum_{i'=2}^{i-1} \mathscr{F}_{i',j} \tag{46}$$

and λ_1 is defined in equation (37). The boundary conditions (42) and (43) require that

$$S^{\eta}_{1,j+1/2} = 0, \quad S^{\eta}_{N^{\eta}+1,j+1/2} = 0,$$

$$t^{\eta}_{1,j+1/2} = 2\frac{\Delta T_2}{\Delta T_1}, \quad t^{\eta}_{N^{\eta}+1,j+1/2} = 0. \tag{47}$$

The two systems of algebraic equations comprising equations (44) and (45) can now be separately solved by following the procedure described in Section 4.1, where convergence is said to have been achieved when the absolute error between successive approximations for $S^{\eta}_{i,j+1/2}$ and $t^{\eta}_{i,j+1/2}$ reach values less than some tolerances ε_3^1 and ε_3^2, respectively.

4.3. *Numerical solution for* $\tau_n^* < \tau < \infty$

At large times the solutions for the non-dimensional streamfunction $f(\eta, \tau)$ and the temperature function $\theta(\eta, \tau)$ are known to approach the steady state profiles $f(\eta, \infty)$ and $\theta(\eta, \infty)$ associated with the constant temperature difference ΔT_2 at the plate. The solutions of the ordinary differential equations governing this second steady state can be obtained as similarity solutions of equations (10)–(12), from which it can be shown that

$$f(\eta, \infty) = R^{1/4} f_0(\eta R^{1/4}), \quad \theta(\eta, \infty) = R\theta_0(\eta R^{1/4}). \tag{48}$$

The numerical solution described in Sections 4.1 and 4.2 eventually breaks down at time $\tau = \tau_n^*$ because of the coefficients of $\partial^2 f/\partial\eta\,\partial\tau$ and $\partial\theta/\partial\tau$ become small and are tending to negative values in part of the boundary-layer. The matching of the steady state solution (48) at large times with that which is valid at $\tau = \tau_n^*$ is now achieved using an adaptation of the method of Dennis [18].

It is convenient to write the governing equations (7) and (8) in the form

$$\frac{\partial f}{\partial \eta} = \mathscr{F} \tag{49}$$

$$\frac{\partial^2 \mathscr{F}}{\partial \eta^2} + p\frac{\partial \mathscr{F}}{\partial \eta} - \frac{1}{2}\mathscr{F}^2 + \theta = q\frac{\partial \mathscr{F}}{\partial \tau} \tag{50}$$

$$\frac{1}{Pr}\frac{\partial^2 \theta}{\partial \eta^2} + p\frac{\partial \theta}{\partial \eta} = q\frac{\partial \theta}{\partial \tau} \tag{51}$$

where

$$p(\eta, \tau) = \frac{3}{4}f - \frac{1}{2}\tau\frac{\partial f}{\partial \tau}, \quad q(\eta, \tau) = 1 - \frac{1}{2}\tau\mathscr{F} \tag{52}$$

and $q(\eta, \tau) > 0$ for all η when $\tau < \tau_p^*$.

The system of equations (49)–(52) must now be solved subject to the boundary conditions that the solution must coincide with that obtained by the step-by-step marching method at $\tau = \tau_n^*$, and that at some large but finite time $\tau = \tau_\infty$ the solution is given by the steady state analysis. The value of τ_∞ may be varied, but must be taken to be large enough for any further increase to have a negligible effect on the whole solution for $\tau_n^* < \tau < \tau_\infty$. Thus the complete set of boundary conditions is given by

$$\mathscr{F}(\eta, \tau_n^*) = \mathscr{F}_n^*(\eta), \quad \theta(\eta, \tau_n^*) = \theta_n^*(\eta)$$

$$f(\eta, \tau_\infty) = R^{1/4} f_0(\eta R^{1/4}), \quad \mathscr{F}(\eta, \tau_\infty) = R^{1/2} f_0'(\eta R^{1/4}),$$

$$\theta(\eta, \tau_\infty) = R\theta_0(\eta R^{1/4})$$

$$f(0, \tau) = 0, \quad \mathscr{F}(0, \tau) = 0, \quad \theta(0, \tau) = R, \quad \tau_n^* \leqslant \tau \leqslant \tau_\infty$$

$$\mathscr{F}(\eta_\infty, \tau) = 0, \quad \theta(\eta_\infty, \tau) = 0, \quad \tau_n^* \leqslant \tau \leqslant \tau_\infty. \tag{53}$$

A rectangular finite-difference grid with sides parallel to the η and τ directions is constructed using n spatial and m temporal grid intervals and corresponding grid sizes $\tilde{h} = \eta_\infty/n$ and $\tilde{k} = (\tau_\infty - \tau^*)/m$, respectively. A finite-difference approximation to equations (50) and (51) is then achieved by replacing η derivatives by central-differences and the τ derivatives $\partial\mathscr{F}/\partial\tau$ and $\partial\theta/\partial\tau$ by either a backward or forward difference depending on whether $q(\eta, \tau) > 0$ or $q(\eta, \tau) < 0$, respectively. This formulation, using backward or forward differences, ensures that the matrix problem associated with our system of equations, along a line of constant τ, remains diagonally dominant, in the sense described by Varga [21], and enables a convergent solution to be achieved using standard iterative techniques. Thus, equations (50) and (51) become

$$\left(1 + \frac{1}{2}\tilde{h}p_{i,j}\right)\mathscr{F}_{i+1,j} + \left(1 - \frac{1}{2}\tilde{h}p_{i,j}\right)\mathscr{F}_{i-1,j} - \left(2 + \frac{\tilde{h}^2}{\tilde{k}}|q_{i,j}| + \frac{1}{2}\tilde{h}^2\mathscr{F}_{i,j}\right)\mathscr{F}_{i,j} + \tilde{h}^2\theta_{i,j} = \frac{\tilde{h}^2}{\tilde{k}}q_{i,j}\mathscr{F}^*_{i,j} \tag{54}$$

$$\left(\frac{1}{Pr} + \frac{1}{2}\tilde{h}p_{i,j}\right)\theta_{i+1,j} + \left(\frac{1}{Pr} - \frac{1}{2}\tilde{h}p_{i,j}\right)\theta_{i-1,j} - \left(\frac{2}{Pr} + \frac{\tilde{h}^2}{\tilde{k}}|q_{i,j}|\right)\theta_{i,j} = \frac{\tilde{h}^2}{\tilde{k}}q_{i,j}\theta^*_{i,j} \tag{55}$$

for $2 \leqslant i \leqslant n$ and $2 \leqslant j \leqslant m$, where $\mathscr{F}^*_{i,j}$ and $\theta^*_{i,j}$ are defined by

$$\mathscr{F}^*_{i,j} = \mathscr{F}_{i,j+1}, \quad \theta^*_{i,j} = \theta_{i,j+1} \quad \text{if } q_{i,j} < 0 \tag{56}$$

and

$$\mathscr{F}^*_{i,j} = -\mathscr{F}_{i,j-1}, \quad \theta^*_{i,j} = -\theta_{i,j-1} \quad \text{if } q_{i,j} > 0$$

and $\mathscr{F}_{i,j} = \mathscr{F}((i-1)\tilde{h},\ \tau_n^* + (j-1)\tilde{k})$ $\theta_{i,j} = \theta((i-1)\tilde{h},\ \tau_n^* + (j-1)\tilde{k})$. Furthermore, the boundary conditions (53) require that

$$\mathscr{F}_{i,1} = \mathscr{F}_n^*((i-1)\tilde{h}), \quad \theta_{i,1} = \theta_n^*((i-1)\tilde{h}), \quad 1 \leqslant i \leqslant n+1$$

$$f_{i,m+1} = R^{1/4} f_0((i-1)\tilde{h}R^{1/4}),$$

$$\mathscr{F}_{i,m+1} = R^{1/2} f_0'((i-1)\tilde{h}R^{1/4}),$$

$$\theta_{i,m+1} = R\theta_0((i-1)\tilde{h}R^{1/4}), \quad 1 \leqslant i \leqslant n+1$$

$$f_{1,j} = 0, \quad \mathscr{F}_{1,j} = 0, \quad \theta_{1,j} = R, \quad 1 \leqslant j \leqslant m+1$$

$$\mathscr{F}_{n+1,j} = 0, \quad \theta_{n+1,j} = 0, \quad 1 \leqslant j \leqslant m+1. \quad (57)$$

To start the iterative scheme we must prescribe initial values of f, $\mathscr{F}$ and θ throughout the solution domain. An approximation to $f(\eta, \tau_n^*)$ is achieved by integrating equation (49) using the quadrature formulae following from the trapezium rule. Thus initial values of f, $\mathscr{F}$ and θ can be assumed such that they follow a linear variation from the solutions at $\tau = \tau_n^*$ to $\tau = \tau_\infty$. Initial approximations for the functions p and q follow from equation (52) by using a central-difference for the term $\partial f/\partial\tau$.

The iterative procedure for solving the finite-difference system (54), (55) and (57) now proceeds as follows:

(i) Fix the values of f, p and q throughout the domain and perform one complete sweep of the system (54), (55) and (57) to calculate the new values of $\mathscr{F}$ and θ. At each point of the domain $\mathscr{F}_{i,j}$ satisfies a quadratic equation which can be solved exactly using the updated value for $\theta_{i,j}$. The grid points are swept along lines of constant τ in the increasing η direction, starting from $\tau = \tau_n^* + \tilde{k}$ and finishing at $\tau = \tau_\infty - \tilde{k}$. To increase the rate of convergence a successive under-relaxation procedure was employed with relaxation factor ω.

(ii) Integrate the differential equation (49) step-by-step along each line of constant τ, using quadrature formulae based on the trapezium rule.

(iii) Using central differences to approximate the derivative $\partial f/\partial\tau$, values of p and q are re-calculated throughout the domain.

(iv) Continue to perform steps (i)–(iii) until convergence, i.e. until the average of the absolute difference in each of $\mathscr{F}$ and θ over the domain between successive iterations fall below the prescribed tolerances ε_5^1 and ε_5^2, respectively.

5. RESULTS AND CONCLUSIONS

As mentioned in Section 3, the Nag routine D02HAF was used to solve the coupled ordinary differential equations (10) and (11) subject to the boundary conditions (12). In this numerical procedure an absolute error tolerance must be supplied and the upper range of integration must be specified at some finite value instead of infinity. In all the results presented in this paper a tolerance of 10^{-6} and an end-point of $\eta = 15$ were used as it was found that any further decrease and increase, respectively, of the values did not produce results which showed further significant variation. In the discussion of the results that follows we concentrate on the cases $R = 0.5$ and 2 when the value of the Prandtl number, $Pr = 1$.

5.1. *Results for* $0 < \tau \leqslant \tilde{\tau}_n$

The restriction to a finite dimensional ξ space was achieved by taking $\xi_\infty = 10$. The effect on the numerical scheme of variations from this value of ξ_∞, while keeping h^ξ constant, was investigated and it was concluded that any larger value of ξ_∞ produced results which were indistinguishable from those presented in the figures. Thus, the precise time at which transfer to the method of Section 4.2 takes place is $\tilde{\tau}_p = 0.5625$, taking $\eta_\infty = 15$.

The values of the tolerance ε_1^1, ε_1^2, ε_2^1 and ε_2^2 as individual average errors over the $(N^\xi - 1)$ unknown grid points were taken to be $\varepsilon_1^1 = 10^{-4}$, $\varepsilon_1^2 = 10^{-6}$, $\varepsilon_2^1 = 10^{-7}$ and $\varepsilon_2^2 = 10^{-8}$. More restrictive values of both tolerances were considered and discovered to produce numerical results which did not show any significant variation. The observation that smaller values of ε_1^1 and ε_1^2 produce almost identical results follows from the fact that the iterative solutions of the non-linear systems of algebraic equations (35) and (36) each rapidly approach limiting values and satisfy their convergence criteria after only a few iterations.

The initial time τ_0 and first time increment $\Delta\tau_0$ were taken to be $\tau_0 = 5 \times 10^{-5}$ and $\Delta\tau_0 = 10^{-8}$ in all the calculations presented in this paper. This value of τ_0 was found to be the optimum value for the initial time which produced solutions conforming to the small time evolutions most accurately. Any smaller initial time increment was soon increased after several time steps by the doubling procedure described in Section 4.1 so that subsequent values of $\Delta\tau$ at corresponding times were very similar to those obtained using $\Delta\tau_0 = 10^{-8}$ and therefore smaller values of $\Delta\tau_0$ produced almost identical values for the non-dimensional temperature. For both the ratios $R = 0.5$ and 2, the time step doubling criterion was satisfied 19 times leading to a final time increment of 5.24×10^{-3} at the time $\tau = \tilde{\tau}_n$.

The main source of variation in the solutions for the non-dimensional fluid temperature $\theta(\eta, \tau) = G(\xi(\eta, \tau), \tau)$ and velocity function $\partial f/\partial\eta(\eta, \tau) = \tau(\partial F/\partial\xi)(\xi(\eta, \tau), \tau)$ arise by considering changes in the number of grid spaces N^ξ. It was observed that as N^ξ increased and, consequently, h^ξ decreased, the initial development of the numerical solution approached that of the small time solution. The values of N^ξ considered here were $N^\xi = 200$, 400, 800, 1600 and 3200 with corresponding values of $h^\xi = 0.05$, 0.025, 0.0125, 0.00625 and 0.003125, respectively. A comparison of the values of the non-dimensional skin friction coefficient at the plate $\partial^2 f/\partial\eta^2(0, \tau)$ and the non-dimensional heat transfer on the plate $q_w(\tau)$ are presented in Tables 1(a) and (b), respectively, for each value of N^ξ along with the corresponding small time solutions (28) and (29) at vari-

Table 1. Comparison of the small time solutions with the step-by-step solutions evaluated at the plate for the case $R = 2$, as predicted by different grid spacings in the numerical scheme

Non-dimensional	Numerical solution using $N = N^{\xi} = N^{\eta}$ grid spacings					Small time solution
	$N = 200$	$N = 400$	$N = 800$	$N = 1600$	$N = 3200$	
(a) Skin friction coefficient and the small time solution (28)						
0.0005	0.92074	0.92079	0.92080	0.92080	0.92081	0.92081
0.0050	0.94786	0.94803	0.94807	0.94808	0.94808	0.94809
0.0500	1.03356	1.03410	1.03423	1.03427	1.03427	1.03435
0.1000	1.08528	1.08606	1.08626	1.08630	1.08632	1.08660
0.5000	1.29735	1.29926	1.29974	1.29986	1.29989	1.30713
1.0000	1.43932	1.44113	1.44158	1.44169	1.44172	1.47238
2.0000	1.54510	1.54623	1.54651	1.54658	1.54660	1.70608
(b) Heat transfer and the small time solution (29)						
0.0005	−25.6225	−25.6299	−25.6318	−25.6322	−25.6323	−25.6324
0.0050	−8.3775	−8.3793	−8.3799	−8.3800	−8.3800	−8.3799
0.0500	−2.9248	−2.9254	−2.9256	−2.9256	−2.9256	−2.9242
0.1000	−2.1875	−2.1879	−2.1880	−2.1881	−2.1881	−2.1852
0.5000	−1.2150	−1.2152	−1.2153	−1.2153	−1.2153	−1.1989
1.0000	−1.0048	−1.0049	−1.0050	−1.0050	−1.0050	−1.9652
2.0000	−0.9423	−0.9427	−0.9428	−0.9428	−0.9248	−0.8000

ous values of τ for the case $R = 2$. Table 1(b) illustrates that the numerical solutions for the heat transfer for different mesh sizes vary most at small times when the finest grid produces the best approximation to the small time solution, but for larger times, when the small time solution becomes invalid, the five solutions agree closely. In Table 1(a), the numerical solutions for the skin friction for different meshes initially follow the small time solution, but inaccuracies develop in the coarser grids as time proceeds. A similar behaviour was observed for the case $R = 0.5$ as the mesh size was refined. The solutions for $\theta(\eta, \tau)$ and $\partial f/\partial\eta(\eta, \tau)$ are now continued using the method described in Section 4.2 which completes the step-by-step solution method using the independent variables η and τ.

Figures 1 and 2 show the variation of the profiles of $\theta(\eta, \tau)$ and $\partial f/\partial\eta(\eta, \tau)$, respectively, at various times τ calculated using $h^{\xi} = 0.00625$, for $R = 0.5$ and 2. The slight improvement in accuracy of the numerical solution as a whole is not felt to be justified for the additional computational time required by smaller values of h^{ξ}. By plotting the steady state profiles as predicted by the Nag routine solution of the system of equations (10) and (11) and appropriate similarity solutions, the transition from $\tau = 0$ to $\tau = \infty$ is clearly illustrated. The non-dimensional temperature and velocity function profiles demonstrate that initially the effects of the change in surface temperature of the plate are not felt near the outer edge of the boundary-layer.

The evolution of the non-dimensional skin friction coefficient at the plate $\partial^2 f/\partial\eta^2(0, \tau)$ with time τ is illustrated in Fig. 3 for $R = 0.5$ and 2, where $h^{\xi} = 0.00625$ has again been used. The numerical, transient solution is shown to develop closely following the small time solution (28) and is graphically almost identical when $\tau < 0.6$ and $\tau < 0.3$ for $R = 0.5$ and 2, respectively. Similar tendencies have been observed for the non-dimensional heat transfer on the plate $q_w(\tau)$ and so these figures have not been included here.

5.2. *Results for* $\tilde{\tau}_n < \tau \leqslant \tau_n^*$

The restriction to a finite dimensional η space was achieved by taking $\eta_\infty \approx 15$, where any larger value of η_∞ produced results which were indistinguishable from these presented in the figures. The numerical value of $\eta_\infty = 2\xi_\infty \tilde{\tau}_n^{1/2}$ was calculated to be $\eta_\infty = 14.9206$ for both $R = 0.5$ and 2.

The values of the tolerances as individual average errors over the $(N^{\eta} - 1)$ unknown grid points were taken to be equal to the corresponding tolerances set in Section 5.1, namely $\varepsilon_3^1 = \varepsilon_1^1 = 10^{-4}$, $\varepsilon_3^2 = \varepsilon_1^2 = 10^{-6}$, $\varepsilon_4^1 = \varepsilon_2^1 = 10^{-7}$ and $\varepsilon_4^2 = \varepsilon_2^2 = 10^{-8}$. Furthermore, the number of spatial grid points and final time increment at $\tau = \tilde{\tau}_n$ used in the technique described in Section 4.1 were continued to the method described here, so that $N^{\eta} = 1600$ and $h^{\eta} = \eta_\infty / N^{\eta} \approx 0.00933$. A comparison of the use of different spatial steps is presented in Table 1 for $R = 2$, whereby no significant improvement in accuracy is demonstrated with a reduction in this value for h^{η}.

The time τ_n^*, denoting the largest value of τ reached in the numerical scheme before τ_p^*, defined by equation (30), was found to be approximately $\tau_n^* = 4.9$ and $\tau_n^* = 2.6$ for $R = 0.5$ and 2, respectively. In order to progress the time τ_n^* towards the accurate value τ_p^*, the time increments were systematically reduced in this step-by-step method. Starting with the time increment defined from the time step doubling routine, the time steps were halved when their current values was such as to cause the method to break down if another time step was performed. This process was repeated until the value of the time increment reached $\Delta\tau \approx 5 \times 10^{-3}$. The solution for $\theta(\eta, \tau)$ and $\partial f/\partial\eta(\eta, \tau)$ is now con-

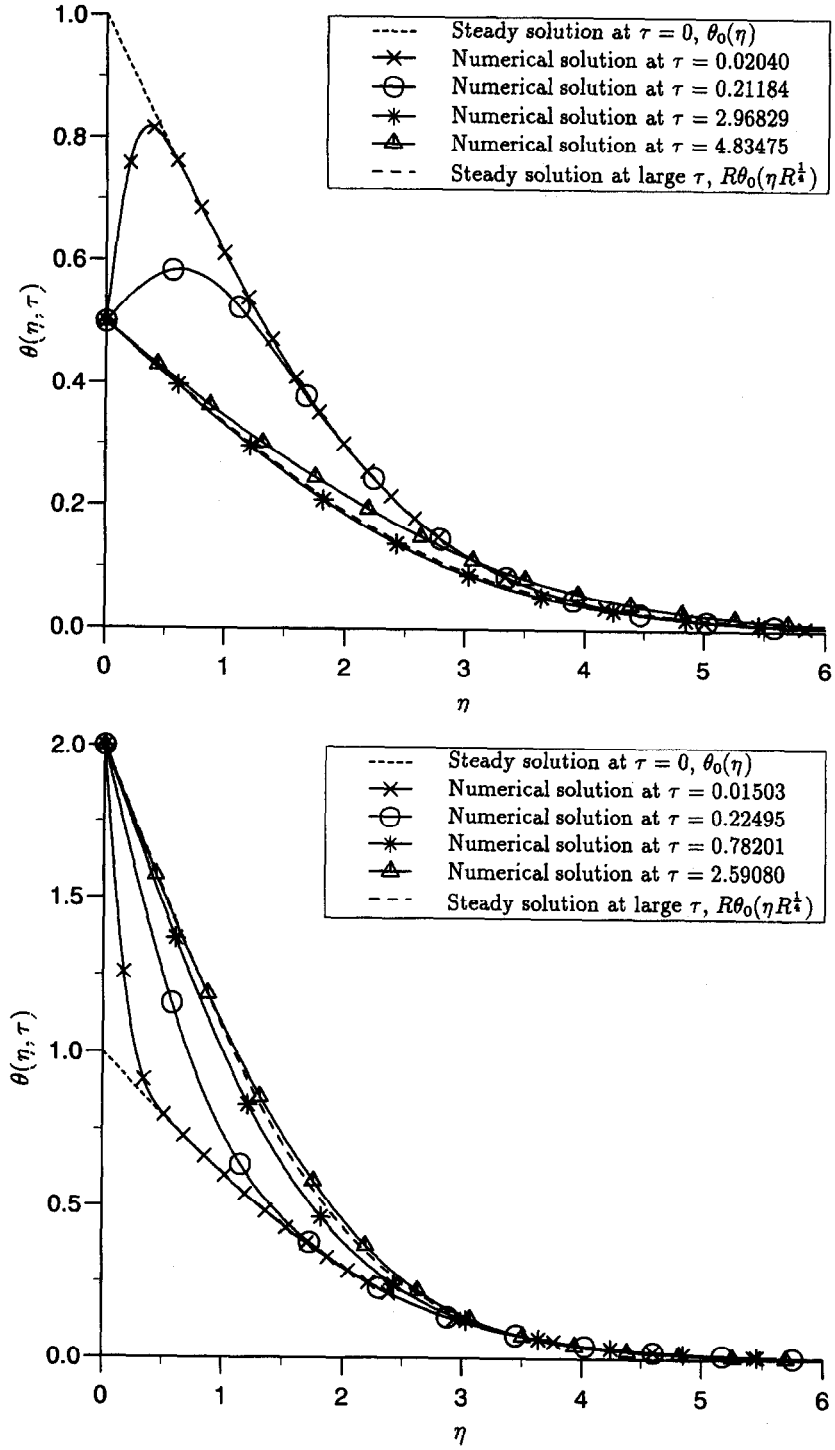

Fig. 1. Variation of the non-dimensional temperature $\theta(\eta, \tau)$ as a function of η at various values of τ and the steady state solutions at $\tau = 0$ and $\tau = \infty$: (a) $R = 0.5$; (b) $R = 2$.

tinued using the method described in Section 4.3 which matches the temperature profile $\theta_n^*(\eta)$ and velocity profile $(\partial f/\partial \eta)_n^*(\eta)$, at which the method described here terminates, to the steady state temperature profiles at $\tau = \infty$.

Figure 3 illustrates that the profiles for the non-dimensional skin friction coefficient at the plate $\partial^2 f/\partial \eta^2(0, \tau)$ approach the steady state solution at $\tau = \infty$, predicted by the similarity solution of the coupled equations (10) and (11), but overshoot and then undershoot slightly before the step-by-step method breaks down. A similar behaviour has also been observed for the non-dimensional heat transfer on the plate $q_w(\tau)$. Furthermore, as time progresses,

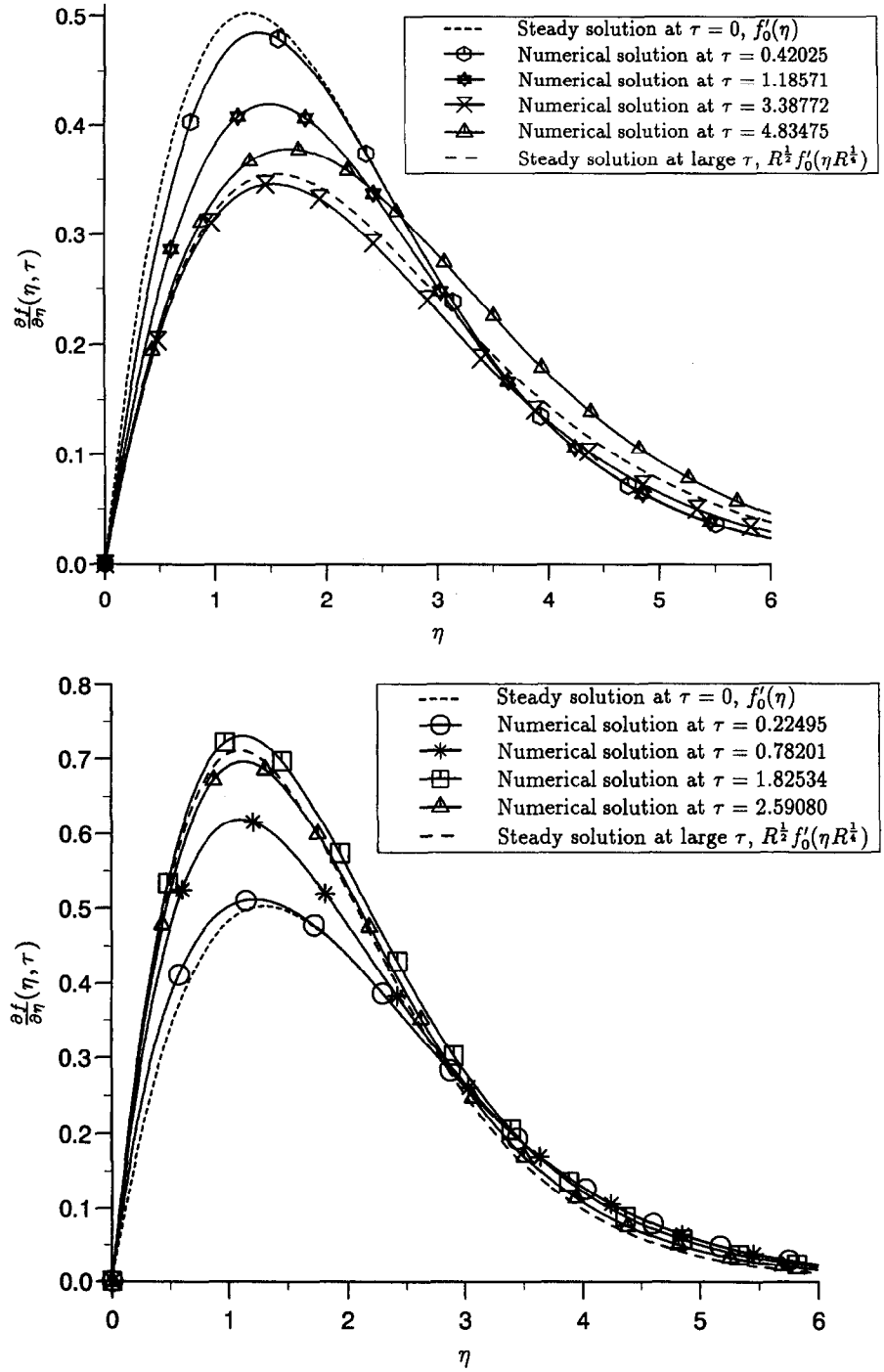

Fig. 2. Variation of the non-dimensional velocity function $\partial f/\partial \eta(\eta, \tau)$ as a function of η at various values of τ and the steady state solutions at $\tau = 0$ and $\tau = \infty$: (a) $R = 0.5$; (b) $R = 2$.

the profiles of temperature, $\theta(\eta, \tau)$, and the velocity function, $\partial f/\partial \eta(\eta, \tau)$, approach and overshoot their predicted values at $\tau = \infty$ near to the plate surface whilst further from the plate a monotonic transition from the values at $\tau = 0$ to $\tau = \infty$ takes place. This effect is most noticeable in the velocity profiles in Fig. 2, but also occurs in the temperature profiles displayed in Fig. 1.

5.3. *Results for* $\tau_n^* < \tau < \infty$

The restriction of the solution domain to finite dimensions is achieved by retaining the value of $\eta_\infty \approx 15$ from Section 5.2 and enforcing the steady state solution to apply at $\tau_\infty = 12$ and $\tau_\infty = 8$ for $R = 0.5$ and 2, respectively. Larger values of the parameters η_∞ and τ_∞ were considered and observed to not significantly affect the final solutions presented

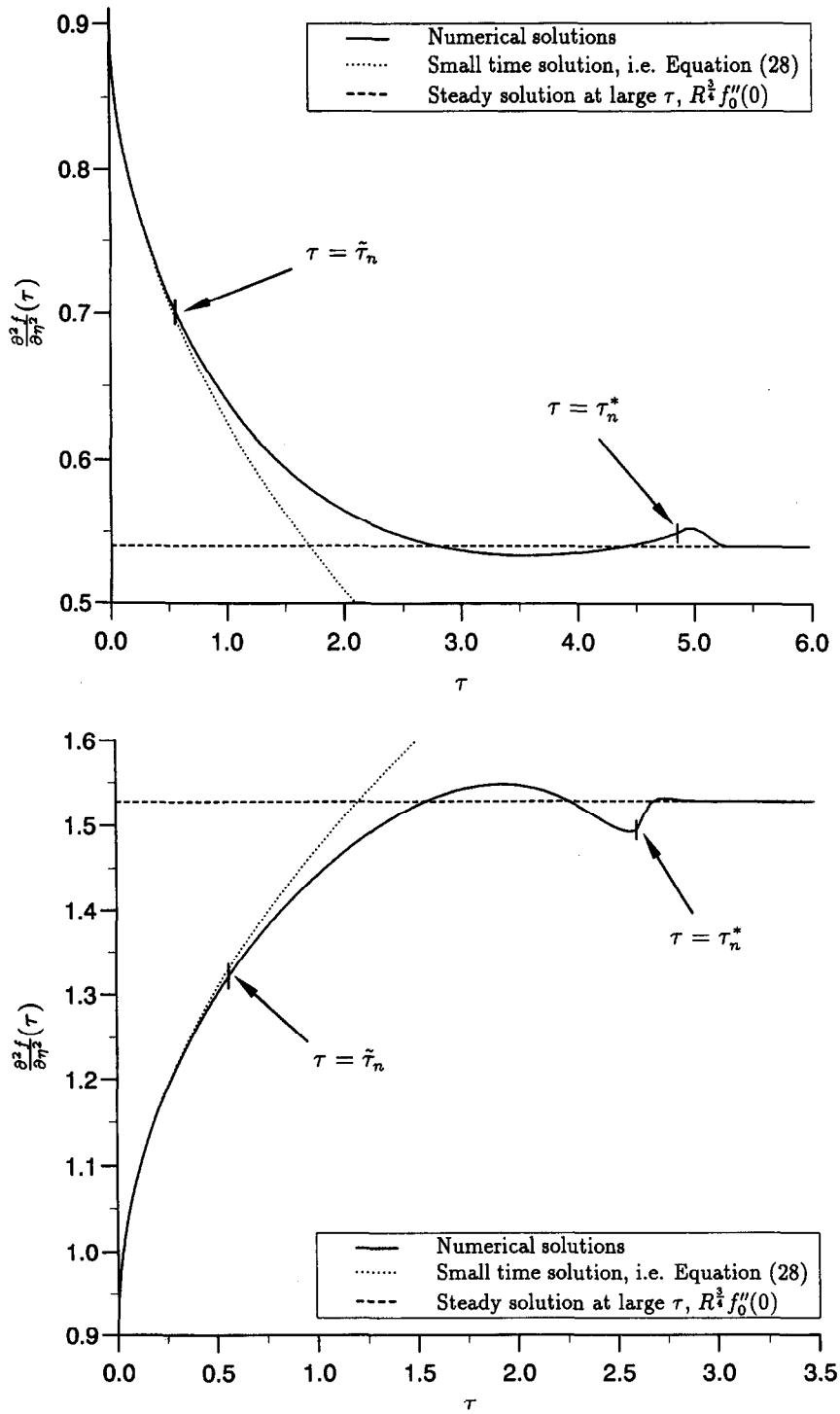

Fig. 3. Variation of the non-dimensional skin friction coefficient at the plate $\partial^2 f/\partial \eta^2(\tau)$ as a function of τ, the small time solution and the steady state solution $\tau = \infty$, where the transition between the solution methods of Sections 4.1, 4.2 and 4.3 occur at the indicated times $\tau = \tilde{\tau}_n$ and τ_n^*. (a) $R = 0.5$; (b) $R = 2$.

in the figures. The convergence criterion was set by assigning the values $\varepsilon_5^1 = 10^{-10}$ and $\varepsilon_5^2 = 10^{-10}$ for the tolerance. These values were shown to produce a numerical solution correct to about five significant figures for those parameters under investigation and had to be made small due to the slow rate of convergence of this method. The use of the relaxation parameter ω was successful in increasing the rate of convergence. The optimum value was found to be the largest value for which the numerical scheme converged and this was in the range $0.5 \leqslant \omega \leqslant 0.7$ for the majority of solutions presented.

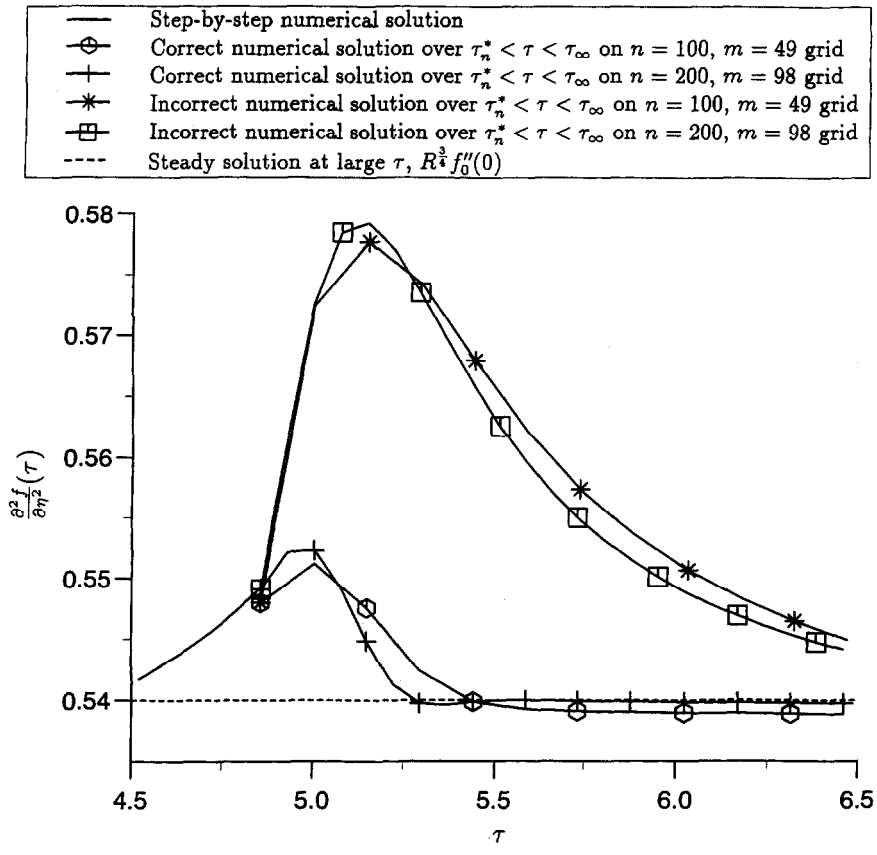

Fig. 4. Variation of the non-dimensional skin friction coefficient at the plate $\partial^2 f/\partial \eta^2(\tau)$ as a function of τ and the steady state solution at $\tau = \infty$. Several different mesh sizes are displayed for each of the two solutions that exist between $\tau = \tau_n^*$ and $\tau = \tau_\infty$. (a) $R = 0.5$, (b) $R = 2$.

Transient numerical solutions for the non-dimensional temperature $\theta(\eta,\tau)$ and velocity function $\partial f/\partial\eta(\eta,\tau)$ were found for the grid spacings $\tilde{h}\approx 0.15$, $\tilde{k}\approx 0.15$ and $\tilde{h}\approx 0.075$, $\tilde{k}\approx 0.075$ for both $R=0.5$ and 2, and $\tilde{h}\approx 0.0375$, $\tilde{k}\approx 0.0375$ for $R=2$, where a suitable value of $m=(\tau_\infty-\tau_n^*)/\tilde{k}$ is chosen to give $\tilde{k}$ as near as possible to the desired value. Other mesh sizes were considered and for the cases in which $\tilde{h}$ and $\tilde{k}$ differed greatly no convergent solution could be obtained. Under the assumption of an initial linear variation for the profiles between $\tau=\tau_n^*$ and $\tau=\tau_\infty$, two different solutions are obtained to the finite-difference system (54), (55) and (57). For coarse grids the profiles of the non-dimensional skin friction coefficient and heat transfer at the plate approached limiting values with refinements in mesh size. A transfer of the solution profiles was then observed to occur for finer grid sizes and a second pair of limiting values for the skin friction coefficient and heat transfer detected. Using these two known solutions for $\theta(\eta,\tau)$, $\mathscr{F}(\eta,\tau)$ and $f(\eta,\tau)$ separately as initial approximations for each of the meshes described above, profiles for the skin friction coefficient and heat transfer at the plate were derived for each of the two solutions.

A comparison of the profiles of the skin friction coefficient at the plate derived from this matching technique are presented in Fig. 4 for both $R=0.5$ and 2. As the mesh size was reduced the numerical solutions were observed to approach limiting values over the solution domain, where the finest grids used for $R=0.5$ and 2 required that $n=200$, $m=98$ and $n=400$, $m=144$, respectively. Again, we do not include the corresponding figures for the heat transfer at the plate as they give very similar information. In each case the two limiting solutions exhibit completely different characteristics. The most distinguishing of these is the behaviour around the time τ_n^*, where one solution for the skin friction coefficient attempts to continue the tendencies observed at the end of the step-by-step method, whilst the skin friction coefficient profiles for the second solution approach discontinuous gradients. The physical implications of the two different profiles are clearly depicted in Fig. 5 for $R=2$ and have similarly been observed for $R=0.5$ using the finest grids for which both completely converged solutions were achieved. The contours of the coefficient $[1-\frac{1}{2}\tau(\partial f/\partial\eta)]$ of $\partial^2 f/\partial\eta\,\partial\tau$ and $\partial\theta/\partial\tau$ for the correct solution match across $\tau=\tau_n^*$. Furthermore, the contour $[1-\frac{1}{2}\tau(\partial f/\partial\eta)]=0$ which divides the regions in which information moves in the directions of increasing τ and decreasing τ lies wholly within the domain $\tau>\tau_n^*$, as expected. The corresponding contour for the incorrect solution are entirely inconsistent across the borderline $\tau=\tau_n^*$ between the two methods of solution. The contour $[1-\frac{1}{2}\tau(\partial f/\partial\eta)]=0$ appears to be attempting to pass to times before $\tau=\tau_n^*$ and, therefore, in this solution information is trying to move across a portion of this boundary to τ values at which the coefficient is known to be positive. Clearly, the first of these two limiting profiles is the one which represents both a solution of the finite-difference equations (54), (55) and (57) and matches the boundary conditions correctly.

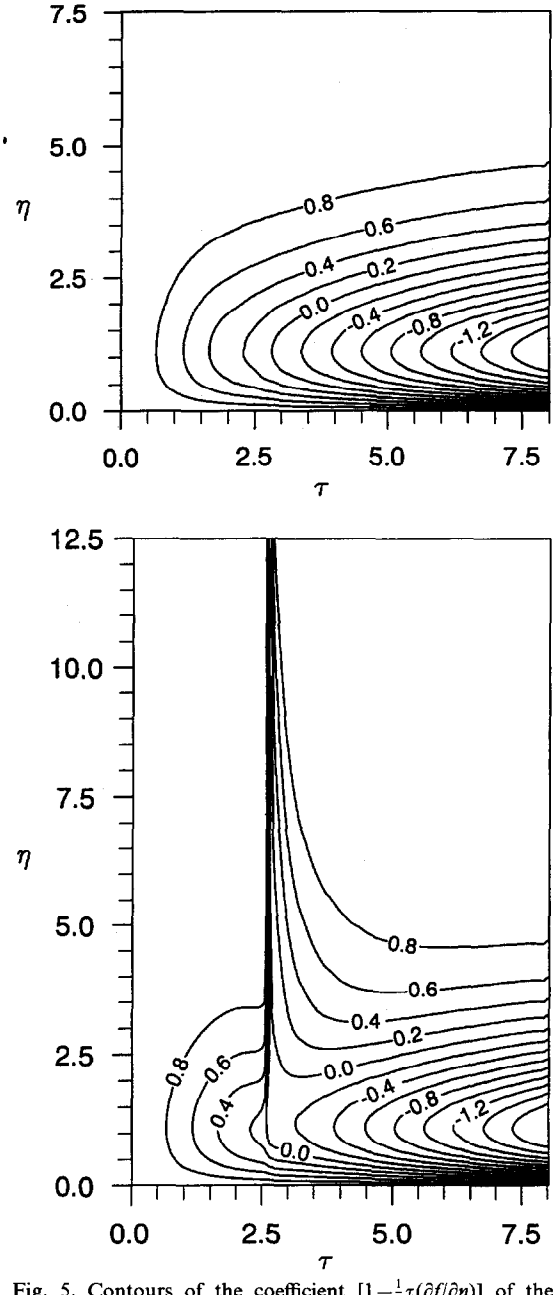

Fig. 5. Contours of the coefficient $[1-\frac{1}{2}\tau(\partial f/\partial\eta)]$ of the expression $\partial^2 f/\partial\eta\,\partial\tau$ and $\partial\theta/\partial\tau$ as a function of τ and η for both numerical solutions when $R=2$ using $\tilde{h}\approx 0.0375$, $\tilde{k}\approx 0.0375$. (a) Physically acceptable solution; (b) incorrect solution.

The determination of the physically acceptable solution becomes progressively more difficult as the grid is refined. For $R=0.5$, both solutions could be achieved for the two coarser grids $\tilde{h}\approx 0.15$, $\tilde{k}\approx 0.15$ and $\tilde{h}\approx 0.075$, $\tilde{k}\approx 0.075$ investigated and the stability of the physically acceptable solution on these grids was confirmed by further reductions of the con-

vergence tolerances by several orders of magnitude. However, for the finer grid $\tilde{h} \approx 0.0375$, $\tilde{k} \approx 0.0375$ when $R = 0.5$, all initial approximations to the correct solution were observed to gradually diverge from this profile and approach the incorrect solution, even with small values of the relaxation parameter $\omega \approx 0.01$. Thus, this acceptable solution appears to become an unstable solution to the finite-difference equations as the mesh size is reduced, so that an initial profile close to this solution may tend to approach the more stable, yet incorrect solution, after a large number of iterations. Similar instabilities in the correct solution were observed for $R = 2$, whereby the acceptable solution could be achieved to any reasonable degree of accuracy for the three mesh sizes described earlier, but for the finer grid $\tilde{h} \approx 0.01875$, $\tilde{k} \approx 0.01875$ all initial profiles converged only towards the incorrect solution.

REFERENCES

1. Illingworth, C. R., Unsteady laminar flow of a gas near an infinite flat plate. *Proceedings of the Cambridge Philosophical Society*, 1950, **46,** 603–619.
2. Sugawara, S. and Michiyoshi, I., Heat transfer by natural convection in the unsteady state on a vertical flat wall. *Proceedings of the 1st Japan National Congress Applied Mechanics*, 1952, pp. 501–506.
3. Siegel, R., Transient free convection from a vertical flat plate. *Transactions of the ASME*, 1958, **80,** 347–359.
4. Hellums, J. D. and Churchill, S. W., Transient and steady state, free and natural convection, numerical solutions: Part 1. The isothermal, vertical plate. *A.I.Ch.E. Journal*, 1962, **8,** 690–692.
5. Carnahan, B., Luther, H. A. and Wilkes, J. O., *Applied Numerical Methods*. Wiley, New York, 1969.
6. Ingham, D. B., Transient free convection on an isothermal vertical flat plate. *International Journal of Heat and Mass Transfer*, 1978, **21,** 67–69.
7. Ingham, D. B., Numerical results for flow past a suddenly heated plate. *Physics of Fluids*, 1978, **21,** 1891–1895.
8. Gebhart, B., Natural convection flows and stability. *Advances in Heat Transfer*, 1973, **9,** 273–348.
9. Gebhart, B., Buoyancy induced fluid motions characteristic of applications in technology. *Journal of Fluids Engineering*, 1979, **101,** 5–28.
10. Joshi, Y., Transient natural convection flows. In *Encyclopaedia of Fluid Mechanics*, Vol. 8, ed. N. P. Cheremisionoff. Gulf, Houston, 1990, pp. 477–533.
11. Pop, I., Ingham, D. B. and Merkin, J. H., Unsteady free and mixed convection in external flows. In *Time-Dependent Nonlinear Convection*, ed. P. A. Tyvand. Computational Mechanics Publications, Southampton, 1997 (to be published).
12. Ingham, D. B., Flow past a suddenly cooled vertical plate. *Journal of the Institute of Mathematics and its Applications*, 1978, **22,** 189–196.
13. Ingham, D. B., Transient mass transfer from an isothermal vertical flat plate. *International Journal of Heat and Mass Transfer*, 1984, **27,** 1837–1843.
14. Joshi, Y. and Gebhart, B., Transient response of a steady vertical flow subjected to a change in surface heating rate. *International Journal of Heat and Mass Transfer*, 1988, **31,** 743–757.
15. Harris, S. D., Ingham, D. B. and Pop, I., Transient free convection from a vertical plate subjected to a change in surface heat flux in porous media. *Fluid Dynamics Research*, 1996, **18,** 313–324.
16. Harris, S. D., Ingham, D. B. and Pop, I., Free convection from a vertical plate in a porous medium subjected to a sudden change in surface heat flux. *Transport in Porous Media*, 1997, **26,** 207–226.
17. Merkin, J. H., Free convection with blowing and suction. *International Journal of Heat and Mass Transfer*, 1972, **15,** 989–999.
18. Dennis, S. C. R., The motion of a viscous fluid past an impulsively started semi-infinite flat plate. *Journal of the Institute of Mathematics and its Applications*, 1972, **10,** 105–117.
19. Ingham, D. B., Flow past a suddenly heated vertical plate. *Proceedings of the Royal Society of London*, 1985, **A402,** 109–134.
20. Burden, R. L. and Faires, J. D., *Numerical Analysis*, 5th edn. PWS, Boston, 1993.
21. Varga, R. S., *Matrix Iterative Analysis*. Prentice-Hall, Englewood Cliffs, New Jersey, 1962.